IOP Publishing Measurement Science and Technology
Meas. Sci. Technol. **28** (2017) 085901 (10pp) https://doi.org/10.1088/1361-6501/aa781b

Experimental calibration procedures for rotating Lorentz-force flowmeters

M G Hvasta[1], **N T Slighton, E Kolemen and A E Fisher**

Princeton University, Princeton, NJ 08544, United States of America

E-mail: MHvasta@princeton.edu

Received 21 March 2017, revised 30 May 2017
Accepted for publication 8 June 2017
Published 14 July 2017

Abstract

Rotating Lorentz-force flowmeters are a novel and useful technology with a range of applications in a variety of different industries. However, calibrating these flowmeters can be challenging, time-consuming, and expensive. In this paper, simple calibration procedures for rotating Lorentz-force flowmeters are presented. These procedures eliminate the need for expensive equipment, numerical modeling, redundant flowmeters, and system down-time. The calibration processes are explained in a step-by-step manner and compared to experimental results.

Keywords: liquid metals, flowmeter, calibration, rotating, Lorentz force

(Some figures may appear in colour only in the online journal)

1. Background and introduction

The rotating Lorentz-force flowmeter was invented by Shercliff in the 1960s [1, 2]. As depicted in figure 1, the flowmeter consists of multiple evenly-spaced permanent magnets that are installed near the rim of a disc-shaped flywheel or magnetic yoke. The center of the magnet assembly is connected to a low-friction bearing that permits rotational motion. When the flowmeter is placed alongside a duct filled with a flowing, electrically-conductive liquid, the resultant Lorentz-force between the liquid and magnets generates a torque upon the flowmeter that causes it to rotate. During operation, the velocity of the liquid within the duct can be determined by measuring the corresponding angular velocity of the flowmeter.

Due to their unique design, rotating Lorentz-force flowmeters (RLFF's) are inexpensive to produce and simple to install. Additionally, because RLFF's are non-contact devices, they are able to operate upon chemically aggressive and/or high-temperature fluids such as molten metals. These features make RLFF's useful instruments that could benefit the nuclear [3, 4], concentrated solar power [5, 6], and metallurgical/casting industries [7, 8].

As previously described by others, the torque generated on the flowmeter is a linear function of the relative velocity between the flowing liquid and the magnets [9, 10]. However, in practice, it is very difficult to calibrate the rotating Lorentz-force flowmeter without: (A) external calibration equipment [7, 9], (B) error-prone analytical or computer modeling [10–12], or (C) redundant flowmeters installed into the flowing system [13, 14]. This paper will outline and experimentally verify procedures that can be used to calibrate RLFF's without any of the aforementioned difficulties or shortcomings.

2. Calibration processes

2.1. Data collection

As shown in figure 1, RLFF's can be rimmed with a number of evenly-spaced, reflective markers. Multiple markers allow an optical tachometer to measure the changes in angular velocity, ω, with greater accuracy and precision than a single marker. A data acquisition system is used to record the values of ω as a function of time. In turn, the data can be analyzed and the measured values of ω can be used to calculate the angular acceleration of the flowmeter, α, according to equation (1):

$$\frac{d\omega}{dt} = \alpha. \tag{1}$$

2.2. Flowmeter torques

When an electrically-conductive fluid moves through a duct made from electrically-insulating, non-magnetic materials the total torque on the flowmeter can be described as:

[1] Author to whom any correspondence should be addressed.

© 2017 Not subject to copyright in the USA. Contribution of U.S. Department of Energy Printed in the UK

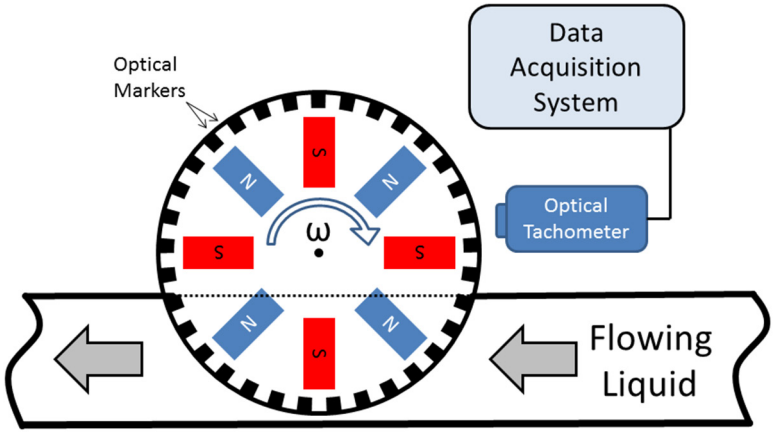

Figure 1. A simple depiction of a Lorentz-force flowmeter setup. The magnet assembly is rimmed with multiple reflective surfaces to enhance data collection. During operation, the magnet assembly rotates about a low-friction bearing located in the center of the disc.

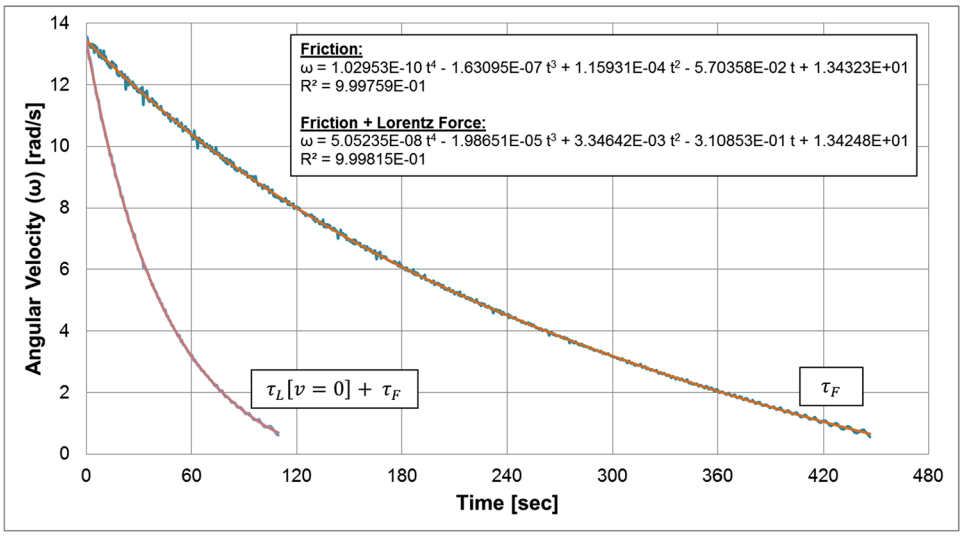

Figure 2. A comparison of the flowmeter deceleration caused by either frictional forces or a combination of both frictional and Lorentz forces. The presence of the liquid metal had a pronounced impact on the deceleration of the rotating flowmeter. As shown above, all data can be accurately modeled using 4th-order polynomial fits. The polynomial fits are only valid for the range of data shown in the plot.

$$\sum \tau = \tau_{\mathrm{L}}\left[v - \omega r\right] + \tau_{\mathrm{F}}\left[\omega\right] = K_{\mathrm{L}}\left(v - \omega r\right) + \tau_{\mathrm{F}}\left[\omega\right] = I\alpha \tag{2}$$

where τ_{L} is the torque generated by the Lorentz-force and τ_{F} is the 'frictional' torque resulting from a combination of friction in the bearings and wind-resistance.

Although the value of the moment of inertia, I, can be experimentally determined after fabrication or accurately calculated using CAD software, it is not required to be known for these calibration processes. Therefore, equation (2) can be re-written as:

$$\frac{K_{\mathrm{L}}}{I}\left(v - \omega r\right) + \frac{\tau_{\mathrm{F}}\left[\omega\right]}{I} = \alpha \tag{3}$$

or

$$\frac{K_{\mathrm{L}}}{I}\left(v - \omega r\right) + \alpha_{\mathrm{F}}\left[\omega\right] = \alpha \tag{4}$$

where

$$\frac{\tau_{\mathrm{F}}\left[\omega\right]}{I} = \alpha_{\mathrm{F}}\left[\omega\right]. \tag{5}$$

If the duct is made from electrically-insulating materials, then τ_{L} is only due to the relative motion between the liquid and the RLFF magnets. Under these conditions, the K_{L} term accounts for all of the magnetic, electrical, and geometric properties of the system. (Historically, the value for K_{L} has been challenging to predict accurately using analytical or numerical methods [2, 10].)

If the duct is made from electrically-conductive materials calculating τ_{L} becomes more complicated for two main reasons. First, the relative motion between the stationary duct and the RLFF magnets will generate additional Lorentz-forces in the system. Second, an electrically-conductive duct provides additional flow paths for the induced electrical currents within the system. Unfortunately, both of these phenomena can affect the motion of the RLFF. However, as noted in Shercliff's original patent [1], the inherent errors caused by using an electrically-conductive duct can be minimized by: (A) ensuring that the duct is more electrically resistive than the liquid ($\sigma_{\mathrm{liquid}}/\sigma_{\mathrm{duct}} \gg 1$), (B) making the duct walls as thin as practical, and (C) installing an electrically-insulating liner on the duct interior.

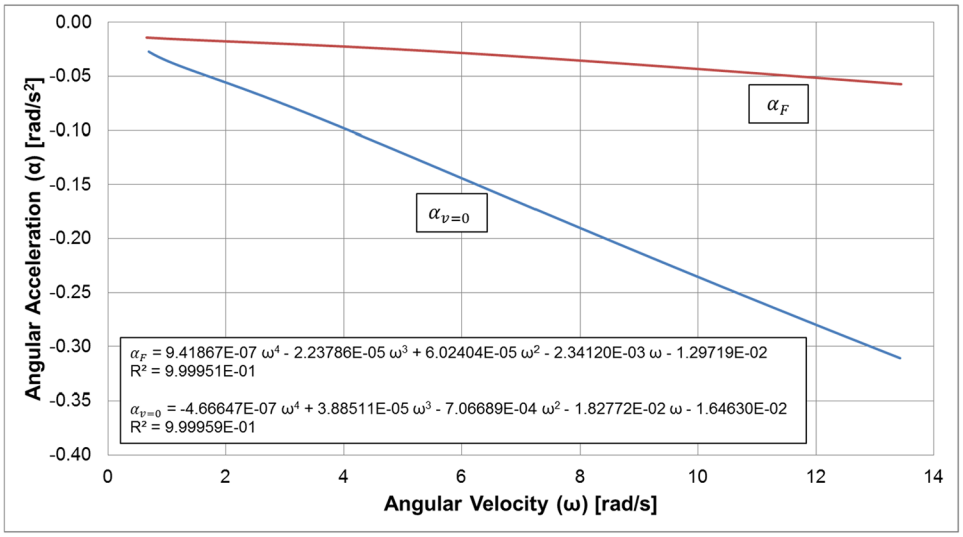

Figure 3. A comparison of the flowmeter deceleration caused by either frictional forces or a combination of both frictional and Lorentz forces.

2.3. Calibration procedure A: 'no-flow' calibration

This calibration procedure can be used if valves or some other mechanism can ensure a 'no-flow' ($v = 0$ (m s^{-1})) condition in the system.

Step A1: Even under ideal conditions it can be challenging to accurately predict frictional losses in bearings [15, 16] and/or windage losses associated with rotating systems [17, 18] using analytical models or numerical simulations. Therefore, the combined effects of frictional and windage losses in the system should be experimentally determined [19]. To experimentally determine the value of $\alpha_{\mathrm{F}}\,[\omega]$, the flowmeter is brought to a location away from the liquid-filled duct so that all Lorentz-forces are eliminated ($\tau_{\mathrm{L}} = 0$ $[N-m]$). The flowmeter should be positioned in the same orientation that it will be in during operation to ensure that frictional losses in the bearings are consistent. Then, the flowmeter is given an initial angular velocity, ω_0. Over time, the frictional losses in the bearings and the windage losses of the system will cause the rotational velocity of the flowmeter to diminish, as shown in figure 2. The data collected during the deceleration of the flowmeter can be used to experimentally calculate the value of $\alpha_{\mathrm{F}}\,[\omega]$.

Step A2: Once the value of $\alpha_{\mathrm{F}}\,[\omega]$ has been measured, the value of $\frac{K_{\mathrm{L}}}{I}$ can be ascertained. To experimentally determine $\frac{K_{\mathrm{L}}}{I}$, the flowmeter must be (re)installed into the system so that it is in operating position next to the liquid-filled duct. The duct should then be isolated or 'valved-off' to prevent bulk flow and ensure that the average liquid velocity, v, is equal to 0 (m s^{-1}). When the flowmeter is again given an initial angular velocity it begins to decelerate more quickly than before, as shown in figure 2. The cause of the faster deceleration is the additional Lorentz-force in the system exerting an extra torque on the flowmeter that opposes rotational motion.

Since the value of $\alpha_{\mathrm{F}}\,[\omega]$ has already been experimentally determined, the value of $\frac{K_{\mathrm{L}}}{I}$ can be accurately calculated using equation (6) and the experimental 'no-flow' angular acceleration data, $\alpha_{v=0}\,[\omega]$, as shown in figures 2 and 3. (During this step in the calibration process a value for the effective radius of the magnets, r, must be assigned. For this paper, r was set equal to the average radius of the magnets.)

$$\frac{K_{\mathrm{L}}}{I}\,(0-\omega r) + \alpha_{\mathrm{F}}\,[\omega] = \alpha_{v=0}\,[\omega]\,. \tag{6}$$

Note that if bulk flow is not prevented using valves or some other mechanism, the relative motion between the fluid and the RLFF magnets could cause the RLFF to act like a 'moving magnet pump' [20, 21]. Depending on the system and the angular velocity of the RLFF, the induced flow could introduce appreciable errors to the calibration process by causing the average fluid velocity to be non-zero.

Additionally, even if bulk flow is prevented, circulation currents could still unduly skew the $v = 0$ (m s^{-1}) calibration data if precautions are not taken. Circulation currents, such as those depicted in figure 4, are caused by inhomogeneities of the Lorentz-force across the duct. These inhomogeneities can be produced by non-uniform magnetic fields (figure 4(A)) and/or geometric factors, such as using magnets that are smaller than the duct (figure 4(B)).

For some liquid-metal systems it may be possible to eliminate circulation currents by freezing the metal in the duct and then correcting for the different electrical properties of the solid and liquid phases prior to operation (see Step A3). For this paper, magnets larger than the duct diameter were used in the RLFF. Accordingly, when a magnet was fully over the duct the net velocity of the liquid metal acting upon the magnet was zero (due to conservation of mass). This helped to minimize the effects of any circulation currents. If magnets smaller than the duct diameter are used to fabricate a RLFF, it may be best to use the procedure detailed in section 2.4 to avoid calibration errors caused by circulation currents.

Step A3: If circulation currents are a major concern or it is impractical to isolate the liquid-filled duct using valves

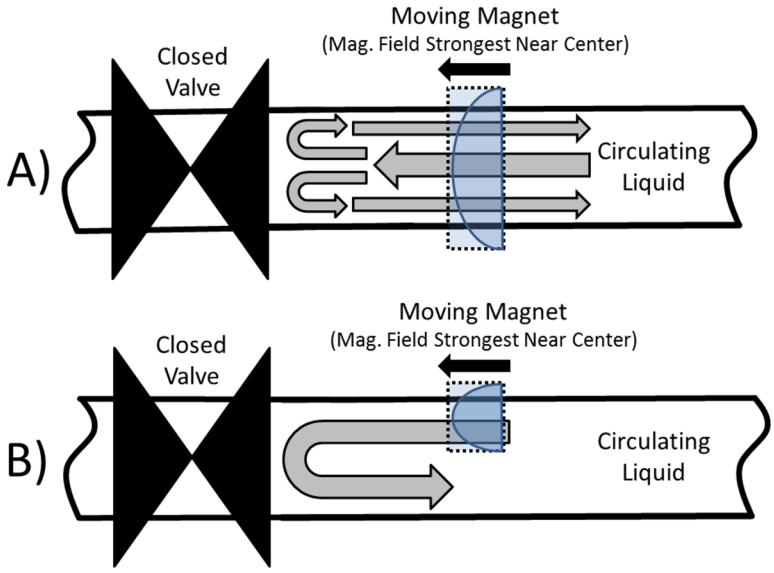

Figure 4. A depiction of 'no-flow' circulation currents. For both conditions shown above, the average velocity in the duct is $v = 0$ (m s^{-1}) but the localized velocities may be non-zero. (A) Circulation currents caused by the non-uniform magnetic field produced by a permanent magnet. (B) Circulation currents caused by the magnet being smaller than the duct.

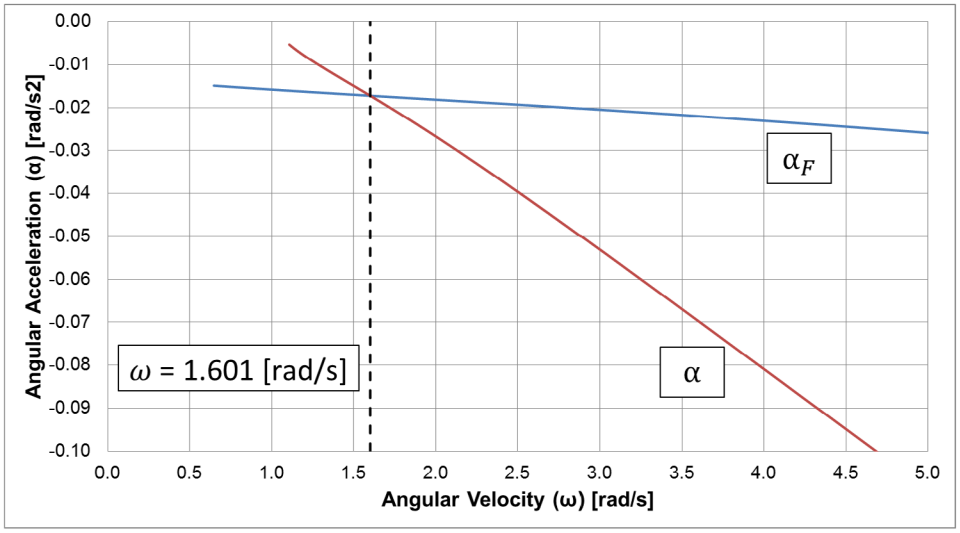

Figure 5. Experimental data showing the intersection of the α and α_{F} plots. For this plot the pump operated at 300 revolutions per minute (RPM). It was determined that the two plots intersected at $\omega = 1.601$ (rad s^{-1}).

or freeze-plugs, the value of $\frac{K_{\mathrm{L}}}{I}$ can be experimentally approximated using a stationary piece of solid metal as a proxy for the liquid [9, 12, 22]. This calibration method yields accurate results so long as: (A) the proxy is in the same geometric configuration as the fluid in the duct, and (B) the experimentally determined value of $\frac{K_{\mathrm{L}}}{I}$ for the proxy is multiplied by the ratio of the electrical conductivities, $\frac{\sigma_{\mathrm{liquid}}}{\sigma_{\mathrm{proxy}}}$.

Step A4: The valve(s) preventing flow can be reopened after the $\alpha_{v=0}[\omega]$ data has been collected. Normal system operation can resume and the average velocity of the fluid can return to $v > 0$ (m s^{-1}).

During steady-state operation the angular acceleration of the system is 0 (rad s^{-2}). Therefore, using the measured angular velocity of the RLFF for a given flow rate and the previous calibration data, the velocity of the liquid can be calculated using any of the following equations:

$$\frac{K_{\mathrm{L}}}{I}(v - \omega r) + \frac{\tau_{\mathrm{F}}[\omega]}{I} = 0 \tag{7}$$

$$v = \omega r - \frac{\alpha_{\mathrm{F}}[\omega]}{\left(\frac{K_{\mathrm{L}}}{I}\right)} \tag{8}$$

$$v = \omega r\left(1 + \frac{\alpha_{\mathrm{F}}[\omega]}{\alpha_{v=0}[\omega] - \alpha_{\mathrm{F}}[\omega]}\right). \tag{9}$$

2.4. Calibration procedure B: flowing operation

The following calibration procedure can be used to acquire accurate, *in situ* data from a RLFF if the flow in the system

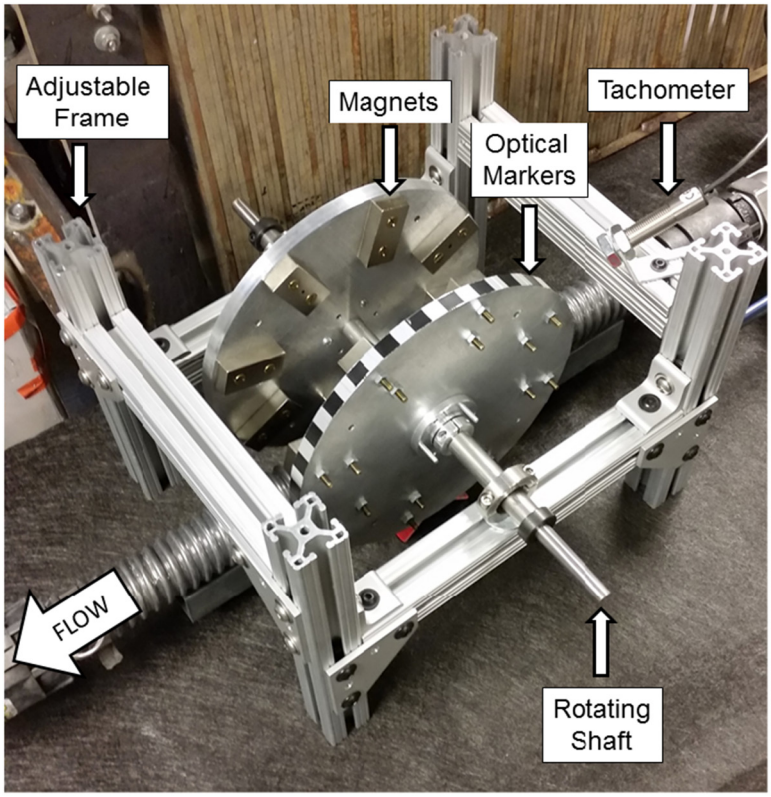

Figure 6. A photo of the rotating Lorentz-force flowmeter used in this experiment.

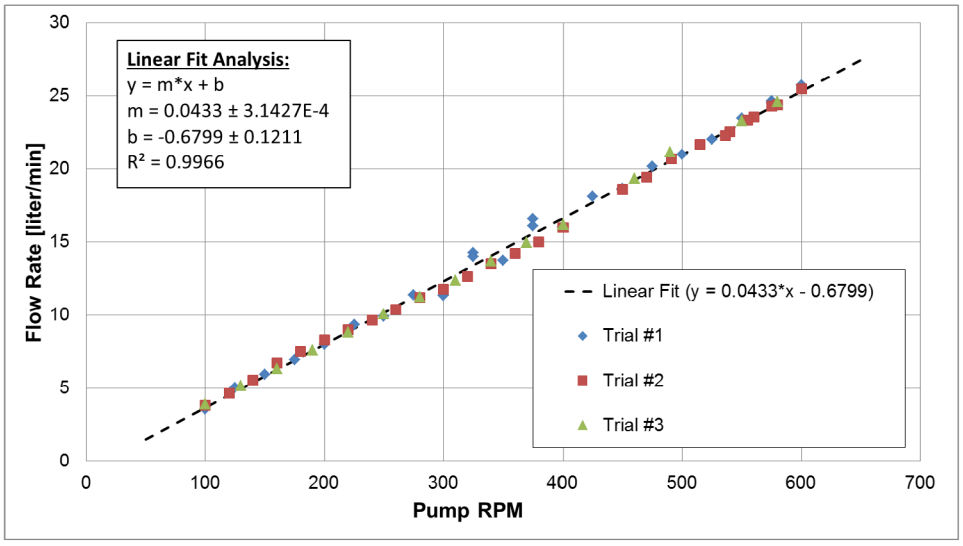

Figure 7. The output of the gear-pump used in LMX. The galinstan flow rate was measured by an Omega FMG96 electromagnetic flowmeter. Error bars (±1%) are omitted from this plot since they fall within the data markers. Uncertainty analysis for the linear fit was performed using the methods outlined in [27, 28].

cannot be stopped to obtain $\alpha_{v=0}\,[\omega]$ data. Moreover, this procedure can be used on fluids with unknown electrical properties or systems that do not lend themselves to being calibrated using a solid proxy (see section 2.3—Step A3).

Step B1: Determine the effective radius, r, of the RLFF magnets. For this experiment the value of r was approximated by averaging the inner and outer radii of the magnets on the RLFF disc. This approximation will become increasingly accurate as: (A) magnet size is reduced, (B) disc diameter is increased ($D/d \gg 1$), and (C) liquid flow is limited to the region near the periphery of the magnet discs.

Step B2: Repeat Step A1 to determine the value of $\alpha_F\,[\omega]$.

Step B3: Once the value of $\alpha_F\,[\omega]$ has been measured, (re)install the RLFF into the system so that it is in operating position next to the flowing, liquid-filled duct. The flowmeter must then be given an initial angular velocity, ω_0, such that $\omega_0 r > v$. Collect angular velocity data and

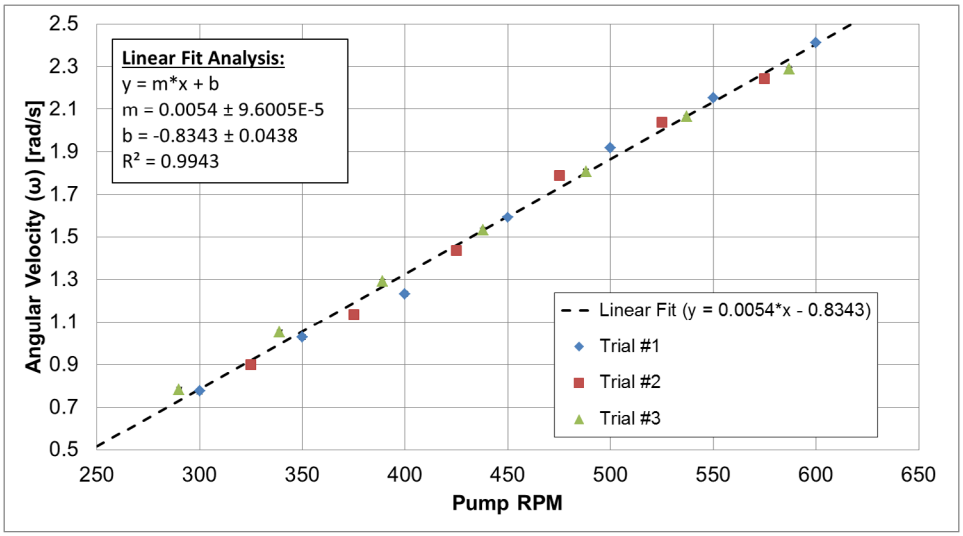

Figure 8. Angular velocity data collected from the continuously operating RLFF. Each data point represents the average of sixty angular velocity measurements. Error bars may be hidden behind the markers but they were calculated according to ISO/IEC Guide 98-3 [29]. Uncertainty analysis for the linear fit was performed using the methods outlined in [27, 28].

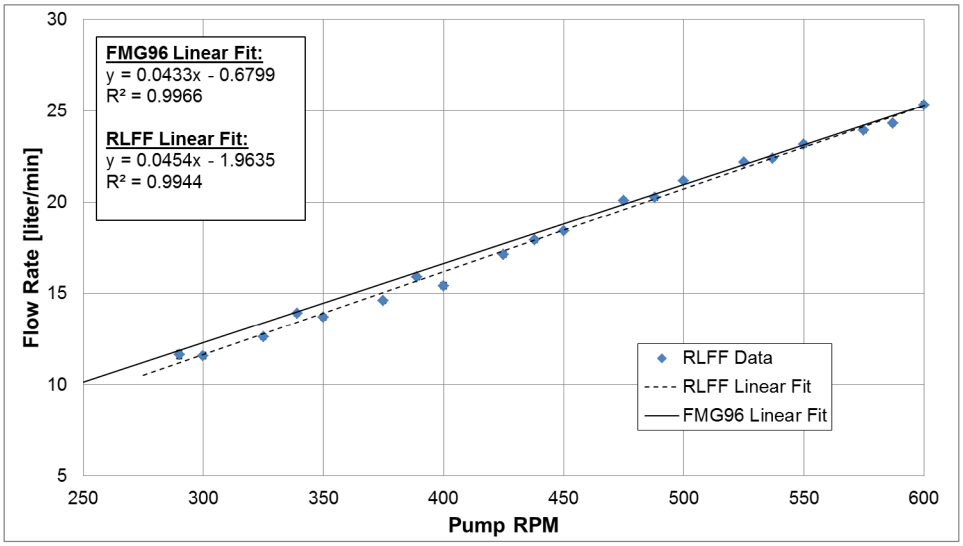

Figure 9. A comparison of the FMG96 and the continuously operating RLFF measurements. The slopes of the linear fits agree to within <5% difference. Error bars may be hidden behind the markers but they were calculated according to ISO/IEC Guide 98-3 [29].

determine the angular acceleration, $\alpha\,[\omega]$, of the disc while the RLFF decelerates and achieves steady-state operation.

Step B4: Analyze the $\alpha_{\mathrm{F}}\,[\omega]$ and $\alpha\,[\omega]$ data to determine the angular velocity at which the two plots intersect, as shown in figure 5. As illustrated by the following equations, when $\alpha_{\mathrm{F}}\,[\omega] = \alpha\,[\omega]$, the $v = \omega r$. Using the previously determined value for r, the velocity of the liquid metal can be calculated. If additional intermittent data is required, Steps B3 and B4 can be repeated as needed.

$$\frac{K_{\mathrm{L}}}{I}\ (v - \omega r) + \ \alpha_{\mathrm{F}}\,[\omega] = \alpha\,[\omega] \tag{10}$$

$$v - \omega r = \frac{\alpha[\omega] - \alpha_{\mathrm{F}}\,[\omega]}{\left(\frac{K_{\mathrm{L}}}{I}\right)} = 0. \tag{11}$$

Step B5: If continuous velocity data is required, the flowmeter can be allowed to coast towards its steady-state angular velocity. Then, using the data collected in Steps B1–B4, the value of $\frac{K_{\mathrm{L}}}{I}$ can be calculated by solving the following simultaneous equations:

$$\begin{aligned} \tfrac{K_{\mathrm{L}}}{I}\ (v - \omega_1 r) &= \alpha\,[\omega_1] - \ \alpha_{\mathrm{F}}\,[\omega_1] \\ \tfrac{K_{\mathrm{L}}}{I}\ (v - \omega_2 r) &= \alpha\,[\omega_2] - \ \alpha_{\mathrm{F}}\,[\omega_2] \end{aligned} \tag{12}$$

where v is assumed to be constant and the values of ω_1 and ω_2 are selected near where $\alpha\,[\omega]$ and $\alpha_{\mathrm{F}}\,[\omega]$ intersect so that 'moving magnet pump' effects are minimized (see section 2.3—Step A2). It can then be shown that:

$$\frac{K_{\mathrm{L}}}{I} = \frac{((\alpha\,[\omega_1] - \alpha_{\mathrm{F}}\,[\omega_1]) - (\alpha\,[\omega_2] - \alpha_{\mathrm{F}}\,[\omega_2]))}{r\,(\omega_2 - \omega_1)}. \tag{13}$$

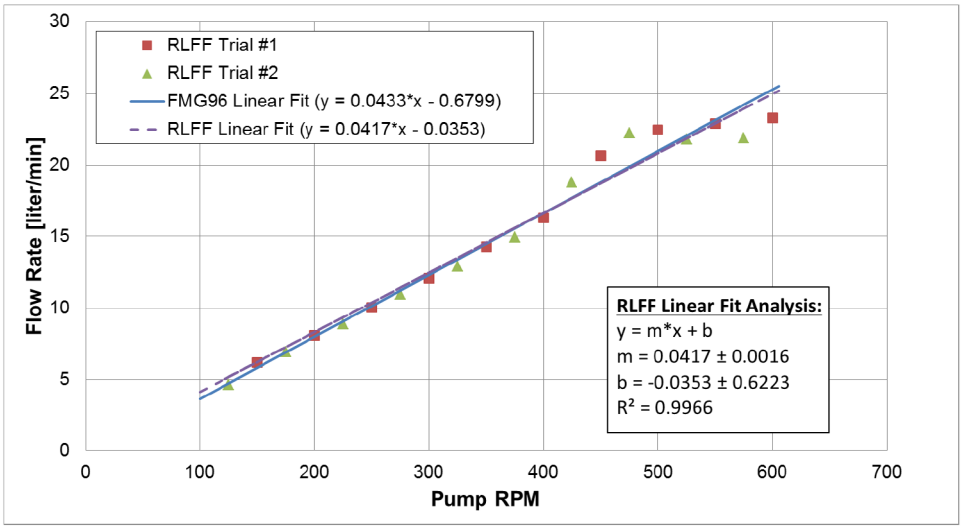

Figure 10. Results of the intermittently operating RLFF compared to the linear fit of the FMG96 data. The average error of all data points on this plot is approximately 4%. The values of $\alpha_F[\omega]$ and $\alpha[\omega]$ were approximated using 4th order polynomial fits. The value of ω was numerically calculated to satisfy $\alpha_F[\omega] = \alpha[\omega]$.

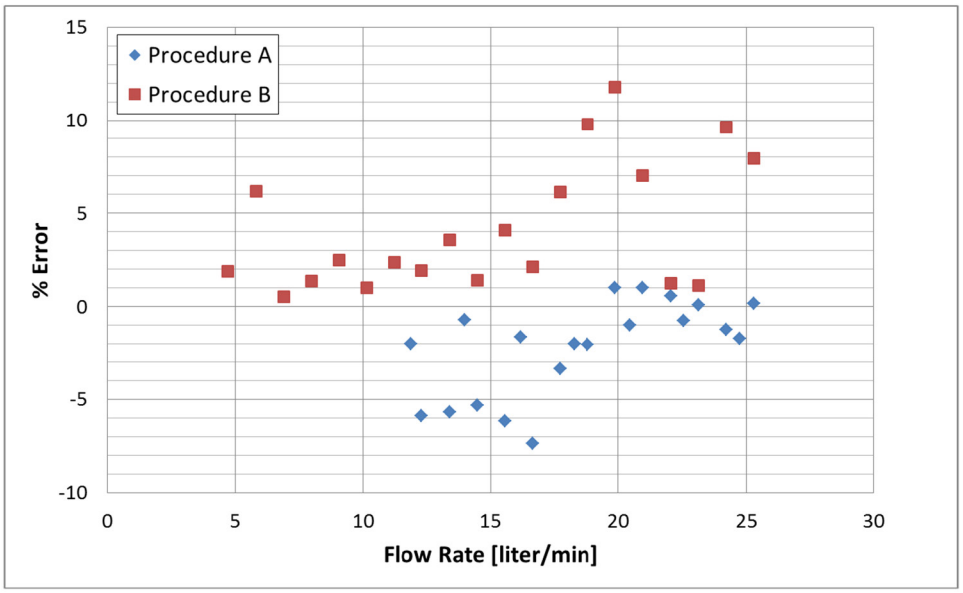

Figure 11. The % error of the different calibration procedures. Most of the data points were within 10% of the commercially available FMG96.

Once $\frac{K_L}{I}$ is calculated, the steady-state operation outlined in 'Calibration Procedure A' can be employed (equations (7)–(9)).

3. Experimental setup

The RLFF calibration was performed within the Liquid Metal eXperiment (LMX) at Princeton Plasma Physics Laboratory [23]. LMX is a closed-loop system that uses a gear-pump to circulate a liquid metal alloy commonly known as galinstan ($Ga^{67}In^{20.5}Sn^{12.5}$ wt.%) through a plastic tubing system ($d = 3.97$ (cm)). The electrical conductivity of galinstan is approximately 3.1E6 ($1/\Omega - m$) [24, 25]. An Omega FMG96 electromagnetic flowmeter was used to measure flow rate through the system in order to verify the RLFF calibration processes. The FMG96 was calibrated and tested using instruments and procedures that are traceable to NIST. The accuracy of the FMG96 was certified to be within $\leqslant 1\%$ of the total flow rate [26].

The RLFF used during this experiment is shown in figure 6. The RLFF used sixteen NdFeB N42 magnets ($5.08 \times 2.54 \times 1.27$ (cm)). These magnets were evenly spaced on to opposing aluminum discs ($D = 25.4$ (cm)) to produce an alternating (N–S–N–S…) magnetic field across the liquid-metal filled tube. Thirty evenly-spaced optical markers were placed along the rim of the disc in order to measure the angular velocity of the disc with an optical tachometer. The tachometer output was collected using a LabVIEW-based data acquisition system. Additional information pertaining to the LabVIEW and pump calibration can be found in appendix A.2.

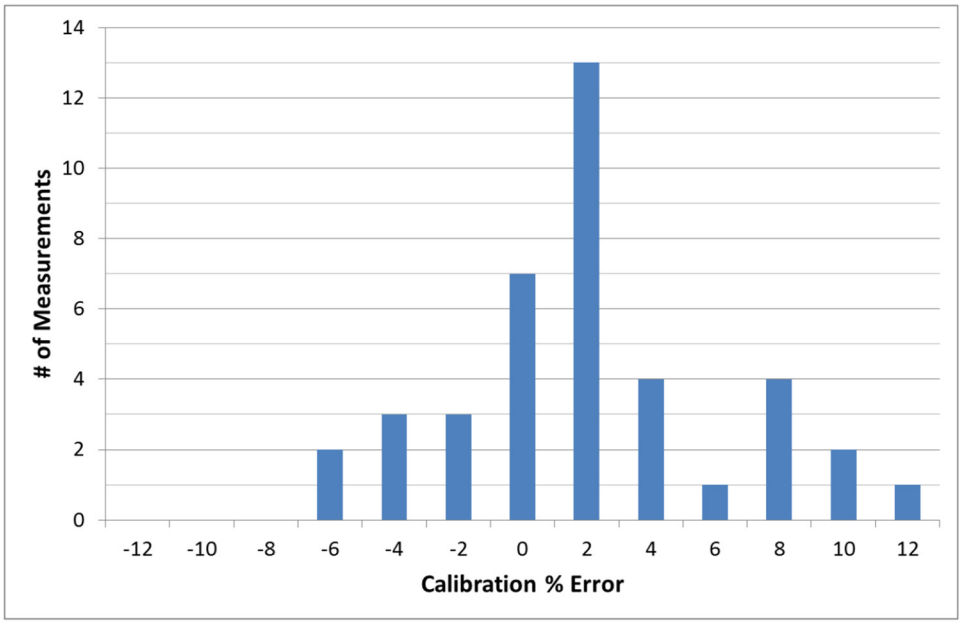

Figure 12. The distribution of calibrated measurement % errors. The majority of calibrated measurements agreed with the commercially available flowmeter to within ~2–3%.

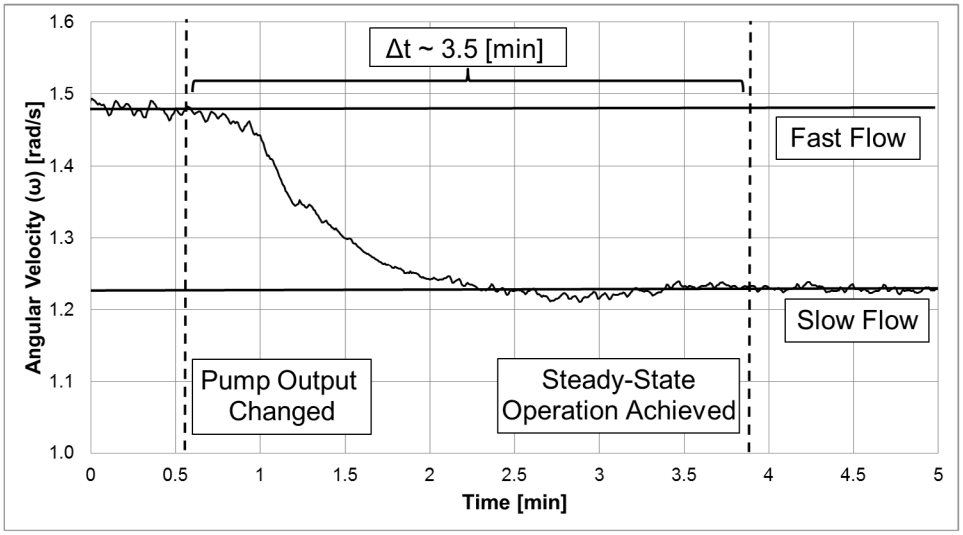

Figure 13. The transient response of the RLFF used in this paper experiencing a sudden change in flow. Experimental data was averaged over a 10 s interval to produce this plot.

4. Experimental results

4.1. Gear-pump output calibration

Due to the nature of gear-pumps, the flow rate was expected to linearly increase with the number of pump revolutions per minute (RPM). As shown in figure 7, the gear-pump behaved as anticipated when the flow rate was measured several times using the commercially available FMG96 electromagnetic flowmeter. The pump was able to produce repeatable outputs over several days of testing.

4.2. Rotating flowmeter operation

4.2.1. Calibration procedure A results. The un-calibrated, steady-state data produced by the RLFF can be found in figure 8. As previously mentioned in section 4.1, the galinstan flow rate increased linearly with pump RPM. Therefore, the angular velocity of the RLFF also responded in a linear fashion to increased pump RPM.

As shown in figure 8, the error-bars on the RLFF were largest at reduced flow rates. It is believed that these larger error-bars are due to imbalanced magnet assemblies and imperfections on the surfaces of the bearings connected to the rotating shaft.

Using the calibration process outlined in section 2.3 and the analyzed data shown in figure 3, the RLFF was able to closely match the FMG96 flowmeter data to within 5%, as shown in figure 9. The experimentally determined value for the $\frac{K_L}{I}$ constant was found to be 0.192 ± 0.006 ($1\ m^{-1}\ s^{-1}$).

The flow rate, Q, was calculated using the following equation:

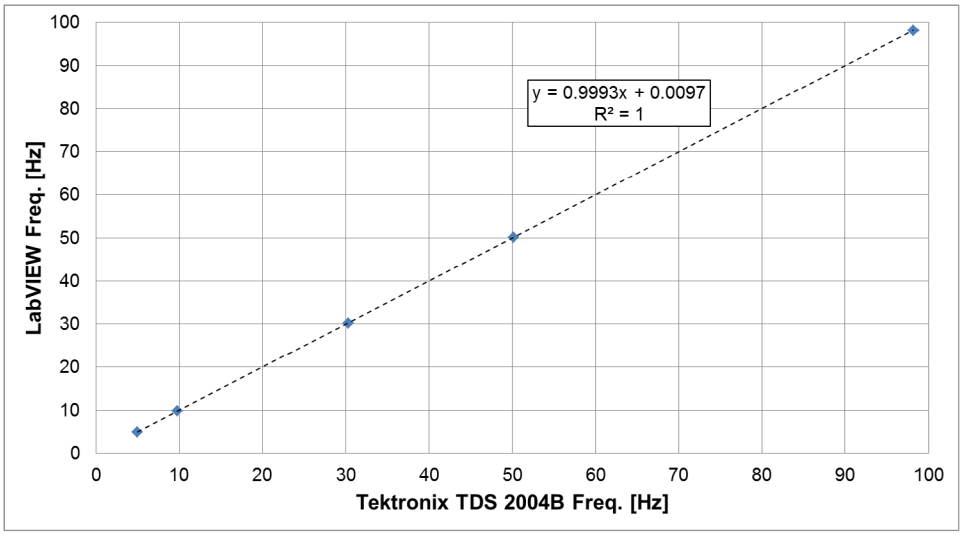

Figure A1. Comparison of frequency measurements performed using the LabVIEW data acquisition setup and a Tektronix oscilloscope. The two devices yielded effectively identical results which demonstrated that the DAQ was functioning properly. The LabVIEW system sampled the binary output of the optical tachometer at a rate of 119–250 (kHz) in order to find the edges of the pulsed output and accurately determine the rotational velocity of the discs.

$$Q = v\left(\frac{\pi d^2}{4}\right). \tag{14}$$

4.2.2. Calibration procedure B results. The RLFF was also operated using the procedure outlined in section 2.4. The effective radius of the magnets was measured to be 10.16 (cm). As shown in figure 10, the intermittent technique (Steps B1–B4) generated data that closely matched the FMG96 flowmeter. Using this calibration method, the average time between measurements was ~10–15 (min).

Using equation (13) and the method outlined in Step B5, the $\frac{K_L}{I}$ constant was calculated to be 0.204 (1 m^{-1} s^{-1}). The small (~5%) discrepancy between this value for $\frac{K_L}{I}$ and the value reported in section 4.2.1 can be attributed to the flowmeter being removed/reinstalled several times during operation and not being returned to the exact same location, which affected the impact of the Lorentz-force on the device.

5. Discussion and future work

Procedures to calibrate a rotating Lorentz-force flowmeter were presented and experimentally verified. Small discrepancies at low flow rates are likely due to imbalances in the magnet discs and imperfections in the bearings that become more apparent at slower angular velocities. As shown in figure 11, nearly all of the measurements from the two calibration procedures described in this paper agreed to within $<10\%$ of the commercially available flowmeter. The majority of the calibrated measurements deviated from the FMG96 by $\leqslant 3\%$ error, as shown in figure 12. It is believed that the slightly unbalanced discs and non-uniform bearing friction caused most of the error in the measurements.

Future work on RLFF's will continue at Princeton University with an emphasis on the following:

(a) The development of advanced, low-friction bearings that promote smaller experimental errors and offer better sensitivity at low flow rates.
(b) Use of advanced materials or novel construction techniques to reduce the overall weight of the RLFF. As shown in figure 13, the continuously operating RLFF requires several minutes to measure sudden changes to steady-state flow. Hopefully, with low-friction bearings and smaller moments of inertia, future RLFF's will respond more quickly to dynamic flow conditions.

Acknowledgments

The authors would like to thank Steven Lowe for his assistance during the fabrication of the flowmeter and Peter Sloboda for his insights regarding LMX upgrades.

The research described in this paper was conducted under the Laboratory Directed Research and Development Program (LDRD) at Princeton Plasma Physics Laboratory, a national laboratory operated by Princeton University for the U.S. Department of Energy under Prime Contract Number: DE-AC02-09CH11466.

This manuscript is based upon work supported by the U.S. Department of Energy, Office of Science, Office of Fusion Energy Sciences, and has been authored by Princeton University under Contract Number DE-AC02-09CH11466 with the U.S. Department of Energy. The publisher, by accepting the article for publication acknowledges, that the United States Government retains a non-exclusive, paid-up, irrevocable, world-wide license to publish or reproduce the published form of this manuscript, or allow others to do so, for United States Government purposes.

The digital data for this paper can be found at:
http://arks.princeton.edu/ark:/88435/dsp01x920g025r

Appendix

A.1. Nomenclature

Variable	Description	Units
d	Duct inner diameter	m
D	Magnet disc diameter	m
I	Moment of inertia	Kg m^2
v	Velocity	m s^{-1}
r	Radius	m
K_L	Lorentz correction factor	N s
α	Angular acceleration	rad s^{-2}
θ	Angular position	rad
σ	Electrical conductivity	1 Ω^{-1} m^{-1}
τ	Torque	N m
ω	Angular velocity	rad s^{-1}
Mathematical convention	Meaning	
$A[x]$	'A' is a function of 'x'	
Abbreviation	Meaning	
LMX	Liquid Metal eXperiment	
RLFF	Rotating Lorentz-force flowmeter	
RPM	Rotations per minute	

A.2. Frequency measurement calibration

A LabVIEW-based data acquisition system was used to measure the output signals of the FMG96 electromagnetic flowmeter and the optical tachometer. To verify that the LabVIEW system was configured correctly, the output from a Wavetek Model 164 function generator was split and connected to both the LabView system and a Tektronix TDD 2004B oscilloscope. As shown in figure A1, the data collected by the LabVIEW system and the oscilloscope agreed very closely. The maximum discrepancy within the range of measurements was found to be 0.07%.

References

[1] Shercliff J A 1960 Improvements in or relating to electromagnetic flowmeters *GB Patent* GB831226

[2] Shercliff J A 1962 *The Theory of Electromagnetic Flow-Measurement* (Cambridge: Cambridge University Press)

[3] Ohshima H and Kubo S 2016 *Sodium-cooled fast reactor Handbook of Generation IV Nuclear Reactors* (Sawston: Woodhead Publishing) ch 5, pp 97–118

[4] Rajan K K, Jayakumar T, Aggarwal P K and Vinod V 2016 Sodium flow measurement in large pipelines of sodium cooled fast breeder reactors with bypass type flowmeters *Ann. Nucl. Energy* **87** 74–80

[5] Lorenzin N and Abanades A 2016 A review on the application of liquid metals as heat transfer fluid in concentrated solar power technologies *Int. J. Hydrog. Energy* **41** 6990–5

[6] Benoit H, Spreafico L, Gauthier D and Flamant G 2016 Review of heat transfer fluids in tube-receivers used in concentrating solar thermal systems: properties and heat transfer correlations *Renew. Sustain. Energy Rev.* **55** 298–315

[7] Kolesnikov Y, Karcher C and Thess A 2011 Lorentz force flowmeter for liquid aluminum: laboratory experiments and plant tests *Metall. Mater. Trans.* B **42B** 441–50

[8] Hernandez D, Schleichert J, Karcher C, Frohlich T, Wondrak T and Timmel K 2016 Local Lorentz force flowmeter at a continuous caster model using a new generation multicomponent force and torque sensor *Meas. Sci. Technol.* **27** 065302

[9] Minchenya V, Karcher C, Kolesnikov Y and Thess A 2011 Calibration of the Lorentz force flowmeter *Flow Meas. Instrum.* **22** 242–7

[10] Buchenau D, Galindo V and Eckert S 2014 The magnetic flywheel flow meter: theoretical and experimental contributions *Appl. Phys. Lett.* **104** 223504

[11] Wang X, Kolesnikov Y and Thess A 2012 Numerical calibration of a Lorentz force flowmeter *Meas. Sci. Technol.* **23** 045005

[12] Alferenok A, Potherat A and Luedtke U 2013 Optimal magnet configurations for Lorentz force velocimetry in low conductivity fluids *Meas. Sci. Technol.* **24** 065303

[13] Thess A, Votyakov E V and Kolesnikov Y 2006 Lorentz force velocimetry *Phys. Rev. Lett.* **96** 164501

[14] Heinicke C 2013 Spatially resolved measurements in a liquid metal flow with Lorentz force velocimetry *Exp. Fluids* **54** 1560

[15] Wang Y, Lin F, Jiang H and Yuan W 2015 Investigation on frictional characteristic of deep-groove ball bearings subjected to radial loads *Adv. Mech. Eng.* **7** 1–12

[16] Knauder C, Allmaier H, Sander D E, Salhofer S, Reich F M and Sams T 2015 Analysis of the journal bearing friction losses in a heavy-duty diesel engine *Lubricants* **3** 142–54

[17] Vrancik J E 1968 *Prediction of Windage Power Loss in Alternators (NASA TN D-4849)* (Cleveland, OH: National Aeronautics and Space Administration)

[18] Zhang Q D, Sundaravadivelu K and Liu N Y 2015 Method for quick prediction of windage power loss *Microsyst. Technol.* **21** 2623–8

[19] Friis Pedersen T 2004 *Characterisation and Classification of RISØ P2546 Cup Anemometer* (Roskilde: Risø National Laboratory)

[20] Baker R S and Tessier M J 1987 *Handbook of Electromagnetic Pump Technology* (Amsterdam: Elsevier)

[21] Hvasta M G 2013 *Designing & Optimizing a Moving Magnet Pump for Liquid Sodium Systems* (Madison, WI: University of Wisconsin Press)

[22] Weidermann C 2012 Design and laboratory test of a Lorentz force flowmeter for pipe flows *PhD Thesis* Technischen Universitat Ilmenau

[23] Hvasta M G, Kolemen E and Fisher A 2017 Application of IR imaging for free-surface velocity measurment in liquid-metal systems *Rev. Sci. Instrum.* **88** 013501

[24] Nornberg M D, Ji H, Peterson J L and Rhoads J R 2008 A liquid metal flume for free surface magnetohydrodynamic experiments *Rev. Sci. Instrum.* **79** 094501

[25] Morley N B, Burris J, Cadwallader L C and Nornberg M D 2008 GaInSn usage in research laboratory *Rev. Sci. Instrum.* **79** 056107

[26] Omega Engineering 2009 *Electromagnetic Flow Meter With PVDF and 316L Construction: FMG90 Series* (Stamford, CT: Omega Engineering)

[27] Hibbert D B 2007 The uncertainty of a result from a linear calibration *Analyst* **131** 1273–8

[28] Origin 2016 (Northampton, MA: OriginLab)

[29] ISO/IEC Guide 98-3 2008 *Uncertainty of Measurement—Part 3: Guide to the Expression of Uncertainty in Measurement (GUM:1995)* (International Organisation for Standardization)